

# Robust Digital Image Watermarking in Curvelet Domain

Peining Tao<sup>a</sup>, Scott Dexter<sup>b</sup>, Ahmet M. Eskicioglu<sup>c</sup>

<sup>a</sup>Dept. of Computer Science, Graduate Center, City University of New York,  
365 Fifth Avenue, New York, NY USA 10016-4309;

<sup>bc</sup>Dept. of Computer Information Science, Brooklyn College, City University of New York,  
2900 Bedford Ave., Brooklyn, NY USA 11201-9642

## ABSTRACT

A robust image watermarking scheme in curvelet domain is proposed. The curvelet transform directly takes edges as the basic representation element; it provides optimally sparse representations of objects along edges. The image is partitioned into blocks and curvelet transform is applied to those blocks with strong edges. The watermark consists of a pseudorandom sequence is added to the significant curvelet coefficients. The embedding strength of watermark is constrained by a Just Noticeable Distortion model based on Barten's contrast sensitivity function. The developed JND model enables highest possible amount of information hiding without compromising the quality of the data to be protected. The watermarks are blindly detected using correlation detector. A scheme for detection and recovering geometric attacks is applied before watermark detection. The proposed scheme provides an accurate estimation of single and/or combined geometrical distortions and is relied on edge detection and radon transform. The selected threshold for watermark detection is determined on the statistical analysis over the host signals and embedding schemes. Experiments show the fidelity of the protected image is well maintained. The watermark embedded into curvelet coefficients provides high tolerance to severe image quality degradation and robustness against geometric distortions as well.

**Keywords:** image watermarking, curvelet domain, JND, radon transform, detection threshold

## 1. INTRODUCTION

Due to the fast and extensive growth of network technology, digital information can be distributed with no quality loss, low cost and nearly instantaneous delivery. Protection of multimedia content has recently become an important issue because of consumers' insufficient cognizance of the ownership of intellectual property. Thus, content owners are eagerly seeking technologies that promise to protect their rights. Two fundamental groups of technologies have been identified with the purpose of discouraging unauthorized consumption and duplication: encryption and watermarking [1,2,3].

Encryption makes multimedia content unintelligible through a reversible mathematical transformation and is probably the most common method of protecting digital content. However, encryption can protect content in transit, but once decrypted, the content has no further protection. Watermarking has been considered to fulfill this need because it embeds data directly into a multimedia element such as an image, audio or video file. In general, a watermarking system must have two characteristics: 1) Perceptual transparency: An embedded watermark should not introduce a significant degree of distortion to the cover image. 2) Robustness: A watermark should be difficult to remove from the watermarked image. It has to survive after the image has undergone some normal signal processing or malicious attacks.

In the past two decades, many research papers proposed to embed watermark in the wavelet transform domain [6,7,8,9] which provides multiresolution representation of the cover work. For one dimensional signal, wavelet transform provides near optimal representation of one dimensional signal with point singularities. However wavelets are not well suitable for detecting, organizing, or providing a compact representation of intermediate dimensional structures, it lost advantages over dealing with two dimensional signal e.g., curves or edges with line singularities [12,13]. A recently introduced family of the curvelet transform was developed in the last few years in an attempt to overcome inherent limitations of traditional multiscale representations. Curvelet transform directly take the edge as the basic representation element; it is anisotropic with strong direction, and provide optimally sparse representations of objects along a general curve with bounded curvature [14,15]. Such representations turn out to be far more sparse than the wavelet decomposition of the object. In fact, it is provable that one can recover such objects from noisy data by simple curvelet

shrinkage and obtain a Mean Squared Error (MSE) order of magnitude better than what is achieved by more traditional methods [14,15].

## 2. CURVELET TRANSFORM

Along with the wavelet transform and the ridgelet [16] transform, the curvelet transform theory is based on sparsity theory [16]. The following two sections summarize the curvelet mathematical transform and digital implementation presented in [12,13,14,15].

### 2.1 Continuous-time curvelet transform

The idea of curvelets is to compute the inner product between the signal or function and the curvelet function to realize the sparse representation of the signal or function. So the curvelet transform can be expressed as

$$c(j, l, k) := \langle f, \varphi_{j,l,k} \rangle \quad (1)$$

here,  $j=0, 1, 2, \dots$  is a scale parameter;  $l=0, 1, \dots$  is an orientation parameter; and  $k=(k_1, k_2) \in Z^2$  is a translation parameter. The waveform  $\varphi_j(x)$  is defined by means of its Fourier transform  $\varphi_j(\omega)=U_j(\omega)$ , where  $U_j$  is frequency window defined in the polar coordinate system such as:

$$U_j(r, \theta) = 2^{-3j/4} W(2^{-j} r) V\left(\frac{2 \lfloor j/2 \rfloor \theta}{2\pi}\right), \quad (2)$$

$W$  and  $V$  are radial and angular windows respectively and will always obey certain admissibility conditions. Curvelets at scale  $2^j$ , orientation  $\theta_l$  and position  $x_k^{(j,l)} = R_{\theta_l}^{-1}(k_1 \cdot 2^{-j}, k_2 \cdot 2^{-j/2})$  can be expressed as:

$$\varphi_{j,l,k}(x) = \varphi(R_{\theta_l}(x - x_k^{(j,l)})) \quad (3)$$

where  $\theta_l = 2\pi \cdot 2^{-\lfloor j/2 \rfloor} \cdot l$ ,  $l=0,1,\dots$ ,  $0 \leq \theta_l < 2\pi$ ,  $R_\theta$  is the rotation by  $\theta$  radians. A curvelet coefficient is then the inner product between an element  $f \in L^2(R^2)$  and curvelet  $\varphi_{j,l,k}$  as:

$$\begin{aligned} c(j, l, k) &:= \langle f, \varphi_{j,l,k} \rangle = \int_{R^2} f(x) \overline{\varphi_{j,l,k}(x)} dx \\ &= \frac{1}{(2\pi)^2} \int \hat{f}(\omega) U_j(R_{\theta_l} \omega) e^{i \langle x_k^{(j,l)}, \omega \rangle} d\omega. \end{aligned} \quad (4)$$

### 2.2 Digital curvelet transform

Digital Curvelet transform is linear and take as input Cartesian arrays of the form  $f[t_1, t_2]$ ,  $0 \leq t_1, t_2 < n$ , which allow the output as a collection of coefficients:

$$c^D(j, l, k) := \sum_{0 \leq t_1, t_2 < n} f[t_1, t_2] \overline{\varphi_{j,l,k}^D[t_1, t_2]}. \quad (5)$$

The implementation referring to as the FDCT (Fast Discrete Curvelet Transforms) via USFFT is detailed in [15]. Briefly, they (1) take the 2D FFT of  $f$  and obtain Fourier samples  $f'$ , (2) resample (or interpolate)  $f'$  for each scale/angle pair  $(j, l)$  to obtain sample values for sheared  $f'$ , (3) multiply the sheared object  $f'$  with the parabolic window  $U_j$  and (4) apply the inverse 2D FFT to collect the discrete coefficients  $c^D(j, l, k)$ .

It is provable that curvelets provide an essentially optimal representation of edges [14]. Such representations turn out to be far more sparse than the wavelet decomposition of the object. Roughly speaking, to represent an edge to squared error  $1/N$  requires  $1/N$  wavelets and only about  $1/\sqrt{N}$  curvelets [14].

### 3. PROPOSED WATERMARKING SYSTEM

In this paper, we proposed a novel watermarking system based on curvelet domain. The framework of watermarking system is depicted in Fig. 1. The image is partitioned into small blocks, the Fast Discrete Curvelet Transform (FDCT) via Unequally-Spaced Fast Fourier Transforms (USFFT) is employed to decompose those block of strong edges into curvelet domain. We embedded the watermark (a pseudo random sequence) into the selected curvelet coefficients. Then the cover image  $I_w$  is reconstructed, distributed to the public and possibly undergone various attacks. The cover image  $I_w^*$  and the secret key are passed to receiver. As usual, the watermarks are blindly detected using a correlation detector. We have included three essential steps to improve the performance of watermarking system: The developed JND model based on Barten's sensitivity function enables highest possible amount of information hiding without compromising the quality of the data to be protected; A scheme relying on radon transform synchronized embedding location allows the system resist against geometric attacks; The detection threshold is computed based on the statistical properties of detection detector to enforce desired false positive rate. Watermarking algorithm and essential steps are described in detail in the following sections.

#### 3.1 Watermark embedding and detection scheme

We use Canny edge function [10] to detect edges of the original image  $I(x,y)$ . The resulting edge map is a binary image  $B=\{b_{ij}\}$ ,  $i=1,2,\dots,N$ ,  $j=1,2,\dots,N$  containing 1 where the edges are detected and 0 else where. A grid of edge strength is produced based on the edge map. We divide the edge map into small blocks each receives edge strength as:

$$e_k = \sum_{i,j}^n b_{ij} \quad (7)$$

where  $n$  is the block size. Since changes in blocks with strong edge strength are less visible to human eyes, we only permit the watermark embedding to the blocks whose edge strength is greater than a selected threshold. An edge index table identifying those embedding blocks is constructed based on the edge strength map and a determined threshold. Fig. 2 shows an example of edge strength map and edge index table with selected threshold  $T_1=100$ .

We apply FDCT-USFFT to those blocks with strong edges and collect curvelet coefficients. We leave out the largest  $n$  terms in the lowest scale to ensure transparency and choose the significant coefficients in the next immediate scale to embed watermark. Then the watermark  $W=\{w_1, w_2, \dots, w_m\}$ , a pseudo random sequence of real numbers having normal

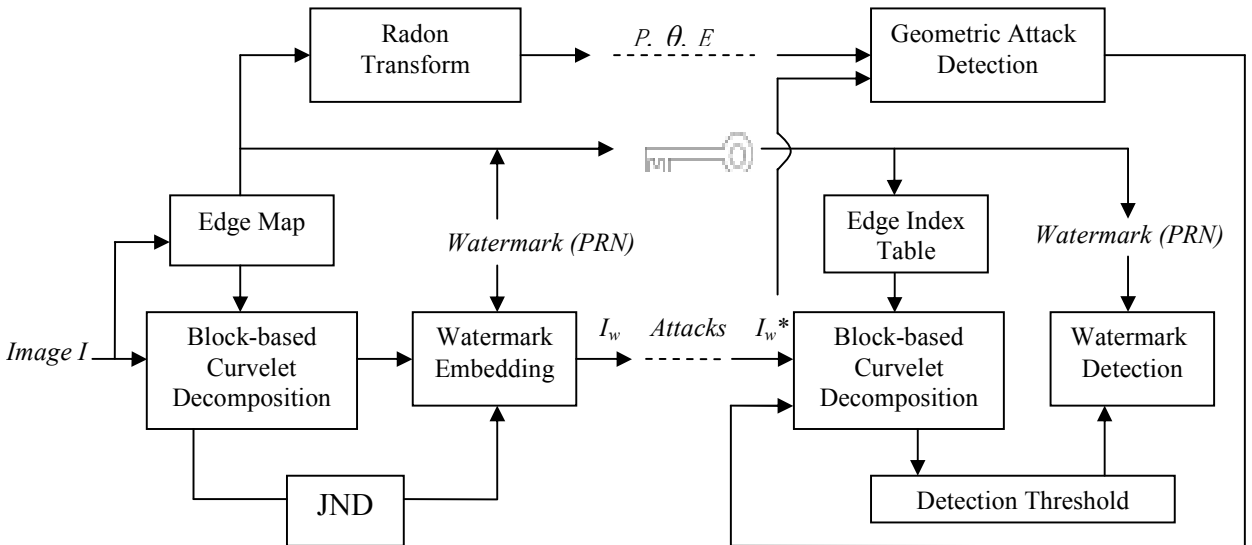


Fig. 1. Framework of proposed watermarking system

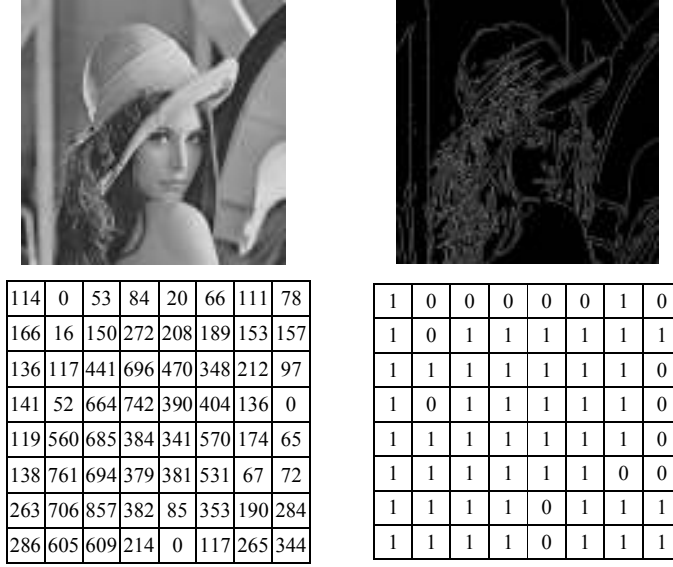


Fig. 2. An example of the edge strength map and the edge index table Up-left: Original image “Lena” Up-right: Edge map of “Lena” under Canny detection Down-left: Corresponding edge strength map with block size 64 Down-right: Edge index table with bit 1 identifying the embedding blocks whose edge strength is greater than 100.

distribution, zero mean and unit variance, is superimposed into curvelet coefficients according to:

$$c_{l,k}^W = c_{l,k} + a \cdot |c_{l,k}| \cdot w_i \quad (8)$$

$a$  is a scaling factor that controls the embedding strength. The determination of the scaling factor is detailed in the next section. The seed value to a random number generator used to generate the watermark is stored in a secret key. The positions of embedding blocks are recorded in an edge index table (see Fig. 2.) The contents in this table are normalized to a binary sequence and saved into the secret key which is required in the detection process. We obtain the modified curvelet coefficients for selected blocks and compute the inverse transform to reconstruct the cover image  $I_w$ .  $I_w$  is distributed to public and possibly undergone various image attacks such as compression, Gaussian noise addition, cropping, rotation, etc.

We evaluate the correlation between watermark and curvelet coefficients to determine whether or not the watermark is present. We split the  $I_w^*$  into  $n \times n$  non-overlapping blocks. The secret key is examined. The edge index table is employed to identify those blocks used for hiding watermark information. We extract coefficients  $[C]^* = \{c_{k,i}^*\}$  with  $k=1,2,\dots,N$  and  $i=1,2,\dots,M$  from  $N$  identified blocks. A detector  $z$  which evaluates the correlation between  $[C]^*$  and the watermark  $W = \{w_1, w_2, \dots, w_j, \dots, w_{m \times n}\}$ , is defined by:

$$z = \frac{1}{NM} \sum_{k=1}^N \sum_{i=1}^M c_{k,i}^* \cdot w_j \quad (9)$$

The embedded watermark yields a response higher than a threshold indicating the cover image is marked. More detail about statistically selecting this threshold for watermark detection is given in the following sections.

### 3.2 JND model

One important issue we considered is the possibility of hiding the highest possible amount of information without affecting the visual quality of the host data. Many approaches have been proposed so far to model the characteristics of the Human Visual System (HVS) [17,18,19,20,21]. A perceptual model generally attempts to account for measuring perceptual variations. It is well known that the response of the HVS varies with the spatial frequency and brightness of its input. Generally, noise is less visible in highly textured regions, edges, dark and bright areas. We developed a novel

perceptual data hiding method in still images based on Barten's (1990) contrast sensitivity function [22]. According to Barten's model, the contrast sensitivity model is a function  $S_c$  of the frequency of the stimulus  $f$  measured in cycles/degree, the orientation of the stimulus  $\theta$  in degrees, the observer viewing angle  $w$  in degrees, and the mean local background luminance  $L_\theta$  in candelas/m<sup>2</sup>. In this paper, we assume the viewing angle and the mean local background luminance to be constants, thus the contrast sensitivity model is becoming a function of two parameters: radial spatial frequency  $\omega$  and orientation in degree  $\theta$ .

The cover image is transformed into curvelet domain and a Just Noticeable Distortion (JND) is computed for each curvelet coefficient. Since the FDCT-USFFT[15] uses some concentric squares to separate scales, there is one such grid per scale and angle. With the increase of the scales, rectangular grids expand along directions and frequency plane. We let  $I_{s,t}^l$  be a grid of curvelet coefficients, where  $s$  denotes the scale parameter while  $t$  denotes the angular parameter and  $l$  denotes the block index. Coefficients with the same scale and angle indices can be grouped together to form a grid of dimension  $m \times n$ . Then the curvelet coefficients grouped together is denoted by  $I_{\omega,\theta}^l = I_{s,t}^l(k_1, k_2)$ , where roughly

$$\omega = s + \frac{k_1}{m} 2^{-j} \quad \theta = t + \frac{k_2}{n} 2^{-j/2} \quad (10)$$

and  $k_1=0,1,\dots,m-1$ ,  $k_2=0,1,\dots,n-1$ . For each block  $B_l$  in cover image, FDCT-USFFT is applied then the curvelet subband coefficients can be denoted by

$$\{I^l(\omega, \theta)\} = \{I_{s,t}^l(k_1, k_2)\} = \text{FDCT-USFFT}\{B_l(x, y)\} \quad (11)$$

The JND profile of each subband curvelet coefficient denoted by  $I_{\omega,\theta}^l$  is established in following steps. Step 1: We define the local contrast in curvelet domain by

$$C_{s,t}^l(k_1, k_2) = \frac{|I(\omega, \theta)|}{\max(I_{s,t}^l(k_1, k_2))^\lambda}, \quad (12)$$

Step 2: We define a novel modulation transfer function (MTF) based on Barten's contrast sensitivity model [22] as:

$$\text{MTF}(\omega, \theta) = \min[S_c(\omega, \theta), S_c(\omega)] \quad (13)$$

Step 3: Then frequency detection threshold of subband image  $I_{s,t}^l$  is determined by

$$T_{s,t}^l = \frac{\iint_{I_{s,t}^l} \omega d\omega d\theta}{\iint_{I_{s,t}^l} \text{MTF}(\omega, \theta) \omega d\omega d\theta} \quad (14)$$

Step 4: Finally, based on the masking function model developed by Scott Daly [24], the JND profile of  $I_{s,t}^l(k_1, k_2)$  is given by

$$\text{JND}(I_{s,t}^l(k_1, k_2)) = T_{s,t}^l \cdot \left( 1 + \left( 0.0153 \left( 392.498 \cdot \left| \frac{C_{s,t}^l(k_1, k_2)}{T_{s,t}^l} \right| \right)^\gamma \right)^4 \right)^{1/4} \quad (15)$$

where  $\gamma$  is a function of texture properties of  $I_{s,t}^l(k_1, k_2)$  in the block  $B_l$  given by

$$\gamma(I_{s,t}^l(k_1, k_2)) = \begin{cases} 1 & \text{if } B_l \in S_1 \\ 0.7 & \text{if } B_l \in S_2 \end{cases} \quad (16)$$

$S_1$  and  $S_2$  are referring to the blocks with weak edges and strong edges respectively. We use Canny edge function to detect edges in cover image. The blocks with strong edge are defined by Equation (7) with edge strength greater than a threshold. Those blocks whose edge strength is less than the threshold are considered as blocks with weak edges. Thus,

$JND(I_{s,f}(k_1, k_2))$  is expected to have lower values in flat areas, whereas textured areas should have higher values. Hence, the watermark sequence  $W=\{w_1, w_2, \dots, w_m\}$  is superimposed into curvelet coefficients and the embedding strength of watermark is limited by  $JND(I_{s,f}(k_1, k_2))$ . When the noise introduced by the watermark is larger than the JND threshold, then the embedding strength is tuned so that the hidden signal is just below the perceptual threshold.

### 3.3 Embedding location synchronization to detect and recover from geometric attacks

A synchronization step to locate the embedded watermark in the content is needed to resist geometric attacks. Our proposed watermarking scheme embeds watermark into blocks with strong edges. Many block-based image watermarking techniques are sensitive to geometric distortions, such as rotation and scaling. This is due to the fact that because of the rotation/scaling there is no more a correspondence between the blocks of the original image and the blocks of the rotated image. Thus the detection of the watermark requires a synchronization step to locate the embedded watermark in the content.

Radon transform (RT) [24] is known to be very robust in detecting alignments; this approach is applied to resist geometric attacks in watermarking application [25]. We propose a method to estimate the geometric distortion based on the edges of the cover images in radon transform. We first obtained a binary edge map and a grid of edge strength as described in previous section. For the purpose of detection of geometric distortion, we only detect the edges within a centered circle, so the edge output will not be affected by rotation or small cropping. We apply radon transform over the edge map which converts the  $x,y$ -representation into a  $\rho, \theta$ -representation,  $\rho$  being a distance of projection from the origin and  $\theta$  is the angle the line makes with the horizontal-axis. If  $f(x,y)$  is an image and  $g(x,y) = f((x/s), (y/s))$  is the image scaled by  $s(s>0)$  in both directions, then the RT of image  $g(x,y)$  is easily found to be :

$$R_g(\rho, \theta) = sR_f\left(\frac{1}{s}\rho, \theta\right) \quad (17)$$

in other words, the RT amplitude of the scaled image is only multiplied by the scale factor  $s$ . If  $f(r, \phi)$  is an image written in polar form and  $g(r, \phi) = f(r, \phi - \phi')$  is the image rotated by  $\phi'$  around the  $(r, \phi)$  coordinate system's origin, then the RT of image  $g(r, \phi)$  is easily determined to be

$$R_g(\rho, \theta) = R_f(\rho, \theta - \phi') \quad (18)$$

The edge map is divided into small blocks as shown in Fig. 3 each receives edge strength defined in Equation (7). A vector  $E(e_1, e_2, \dots, e_k)$  is constructed and normalized with zero mean and unit variance. Thus, the location of main axis  $\theta$ , the max  $\rho$  on the main axis and the normalized  $E$  are reference parameters which are required in watermark detection.

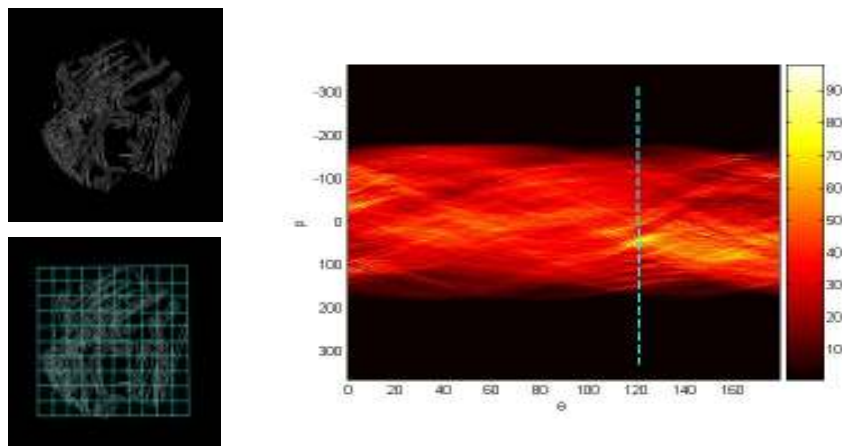


Fig. 3. Left-up: Edge map of 'Lena' within a central circle. Left-down: grid of edge strength. Right: radon transform over edge map with main axis  $\theta=122^\circ$  and  $\rho$  distributed in  $[-180, 181]$ .

Our detector includes an essential step to estimate and compensate the geometric distortion in order to synchronize the location of embedded watermark. Given a corrupted image  $I^*$ , we use the Canny edge function to detect edges. The 2D radon transformation is computed on the edge map of  $I^*$  and we obtain the main axis  $\theta'$  and the max  $\rho'$  on the main axis. Referring to the reference parameters  $[\rho, \theta]$ , we estimate the watermarked image is scaled by the scaling factor  $\rho'/\rho$  and/or rotated by the angle  $\theta' - \theta$ . We invert the image to its original state according to our estimation. Then we divide the edge map  $M^*(x,y)$  into  $n \times n$  blocks each receives edge strength following Equation (7). A vector  $E^*(e^*_1, e^*_2, \dots, e^*_k)$  is constructed and normalized. The auto-correlation, given by

$$\delta = \frac{E^* \cdot E}{\|E^*\| \cdot \|E\|} \quad (19)$$

is calculated to proof check the correctness of distortion estimation. If  $\delta$  is greater than a threshold  $T_2$ , it is indicating the estimation is correct. Hence, we identify and compensate the distortion before applying the detector. If  $\delta$  is less than  $T_2$ , we consider the image has gone through some other affine transforms such as shearing. A heuristic search for the max  $\delta$  is required for accurate estimation.

### 3.4 Detector threshold selection

For correct behavior of the watermark detection system, it is important to properly choose the decision threshold. In the practical watermark decoder, only one of the following situations is possible:

H0: the image is not marked with W;

H1: the image is marked with W.

To discriminate between H0 and H1, the detector computes the correlation value  $z$  in (9) and compares it with a threshold  $T_z$ . If  $z$  is lower than  $T_z$  then the detector decides the image is not marked with  $W$ , whereas if  $z$  is higher than the threshold, the decoder assumes the image is marked with  $W$ . The best value  $T_z$  is the one that minimizing detector error, or the probability of deciding for the wrong hypothesis: the probability of missing the presence of the mark (false negative)  $P(z < T_z | 1)$  and the probability of asserting the presence of W when W is not actually present (false positive)  $P(z > T_z | 0)$ .

As in the typical watermarking scenarios, a vector  $C\{c_1, c_2, \dots, c_N\}$  of curvelet coefficients is selected and the watermark  $W\{w_1, w_2, \dots, w_N\}$  as a pseudo random sequence is additively added to the elements in  $C$ . In watermark detection, a vector  $C^*$  is extracted from curvelet domain of watermarked image  $I^*$ . Therefore, the detector response as the correlation between  $C^*$  and the testing watermark  $\hat{W}$  is:

$$z = \frac{1}{N} \sum_{i=1}^N (c_i \cdot \hat{w}_i + \alpha \cdot |c_i| \cdot w_i \cdot \hat{w}_i) \quad (20)$$

The correlation value  $z$  is a random variable, whose probability density function can be assumed to be Gaussian, in accordance with the central limit theorem; its parameters have been studied with the following hypotheses:  $c_i$  are equally distributed random variables, having symmetrical probability density function and zero mean. If  $N$  is large enough, the watermark here as weight factors  $w_i \in W\{w_1, w_2, \dots, w_N\}$  has the property that different vectors  $W$  and  $\hat{W}$  follows:

$$\frac{1}{N} \sum_{i=1}^N w_i \hat{w}_i = \begin{cases} 1 & \text{if } W = \hat{W} \\ 0 & \text{if } W \neq \hat{W} \end{cases} \quad (21)$$

According to these assumptions, mean of  $z$  can be estimated:

$$\mu_z = \begin{cases} \alpha \mu_{|c|} & \text{if } W = \hat{W} \\ 0 & \text{if } W \neq \hat{W} \end{cases} \quad (22)$$

and variance is

$$\sigma_z^2 \approx \frac{1}{N} \sigma_c^2 \quad (23)$$

for both cases. Experiments show the theoretical estimations for mean and variance are very close to actual experimental ones when  $W \neq \hat{W}$  even when image is under attacks. When  $W \neq \hat{W}$ , the estimation is hardly true because a lot of variables are involved and affect the actual values of  $\mu$  and  $\sigma_z$ . Hence, such considerations are useful to properly choose the decision threshold as:

$$T_z = k \cdot \frac{1}{N} \sqrt{\sum_{i=1}^N c_i^2} \quad (24)$$

where  $k$  is variable which can be turned according to a desired false positive rate given by:

$$P_{fp} = \int_{T_z}^{\infty} P(x) dx = \int_{T_z}^{\infty} \frac{1}{\sqrt{2\pi}\sigma_z} \exp\left(\frac{-x^2}{2\sigma_z^2}\right) dx = \text{erfc}\left(\frac{T_z}{\sigma_z}\right). \quad (25)$$

Observation also shows if we select a false positive  $P(z > T_z) \leq 10^{-7}$ , then the false negative  $P(z < T_z)$  falls between  $10^{-20}$  and  $10^{-30}$  when image is under no attack.

#### 4. EXPERIMENTAL RESULTS

We have tested our proposed watermarking scheme on ten different grayscale images (Lena, Baboon, Boat, Airplane, Goldhill, etc.) of dimension  $512 \times 512$ . They have been partitioned into blocks of  $n' \times n'$  pixels with  $n'=64$ , thus obtaining 64 blocks. We will only give the results for the standard image ‘‘Lena’’. The blocks with edge strength higher than 100 ( $T_1$ ) are selected for watermark embedding. We choose all the significant coefficients in scale 2, the embedding strength is limited by JND threshold. A watermark  $W$  composed of  $m = M \times N$  ( $6144 \times 49$ ) elements is added to curvelet coefficients. The original ‘‘Lena’’, the watermarked ‘‘Lena’’ with PSNR=39.73 and the absolute difference between them are shown in Fig. 4. The fidelity of the image is well maintained because the watermark energy is compacted into noise-unperceivable blocks with strong edges and the introduced distortion is below the just noticeable distortion described in previous section. Fig. 5. shows only the embedded watermark yields a high response far above the threshold and the responds of fake watermarks are all below the threshold. The parameter  $k$  in Equation (24) is determined to be 5.2 to satisfy the requirement of false positive less than  $10^{-7}$ .

We have investigated the robustness of our watermarking system. Take the attack of JPEG compression as example, 1000 watermarks were tested in our experiments. In Fig 6., the response of the detector of the embedded watermark is plotted against JPEG compression with increasing quality factor of the image (from 5% to 90%), along with the detection threshold and the max response of 999 fake watermarks. The detection threshold is obtained by (24) when the factor  $k = 5.2$ . Thus the probability of false positive  $P(z > T_z | \text{the image is not marked with } W)$  is also less than  $10^{-7}$ . Observation shows the embedded watermark survives the severe image compression when the quality factor is 10% and up. Table 2.2 reports the performance of the robustness of our watermarking system against a wide range of image



Fig. 4. Original ‘‘Lena’’, watermarked ‘‘Lena’’ and absolute difference

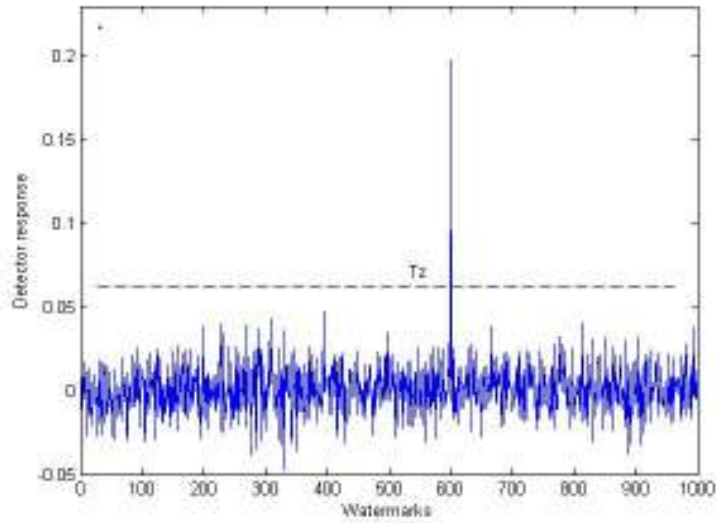


Fig. 5. The detector response of embedded watermark against 999 fake watermarks

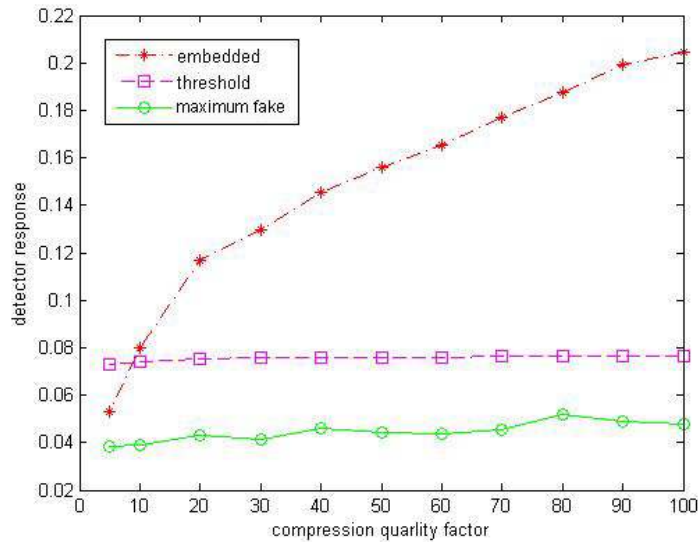


Fig. 6. Detector response of the watermark embedding with JND adjustment is plotted against JPEG compression with increasing quality factor, along with the detection threshold and the maximum response among 999 fake watermarks.

attacks including JPEG compression, Gaussian noise addition, cropping, histogram equalization, contrast adjustment, low pass filtering, Gaussian blur, Gamma correction and sharpening.

The synchronization step in watermarking detection is extremely important because our scheme requires accurate identification of the embedding blocks. Fig. 7. shows a cropped “Lena” rotated by  $30^\circ$  and scaled down by scaling factor 0.75. We compute the radon transform over the edge map of the corrupted “Lena” and obtain the main axis at  $\theta'=152^\circ$  and  $\max(\rho') = 135$ . The vector  $E^*$  is constructed based on (7) where  $n=8$ . Referring to reference parameters, we have  $\theta=122^\circ$  and  $\max(\rho) = 181$ . The distortion is evaluated and the correctness of the estimation is confirmed by  $\delta(0.89) > T_2$  (0.85) defined in (19). We inverted the corrupted watermarked image back to its original state then the detector is applied. The detector response of the embedded watermark is over the threshold with false positive  $\leq 10^{-7}$  and far above all fake watermarks.

Table. 1. Performance of the robustness of our watermarking system against a wide range of image attacks.

Attack	Response of embedded watermark	Maximum fake response	Threshold
No attack	0.1976	0.0478	0.0749
JPEG QF=50	0.1536	0.0434	0.0748
JPEG QF=20	0.1140	0.0418	0.0740
JPEG QF=10	0.0797	0.0390	0.0739
Gaussian noise $v=0.05$	0.2204	0.1309	0.1883
Cropped 50%	0.1318	0.0375	0.0610
Cropped 75%	0.0479	0.0314	0.0478
Gaussian Blur (5x5)	0.1635	0.0413	0.0680
Low pass filtering (3x3)	0.0991	0.0343	0.0578
Histogram Equalization	0.2935	0.0718	0.1149
Gamma correction	0.1949	0.0482	0.0748
Contrast adjustment	0.2340	0.0584	0.0926
Sharpening	0.4891	0.1039	0.1446

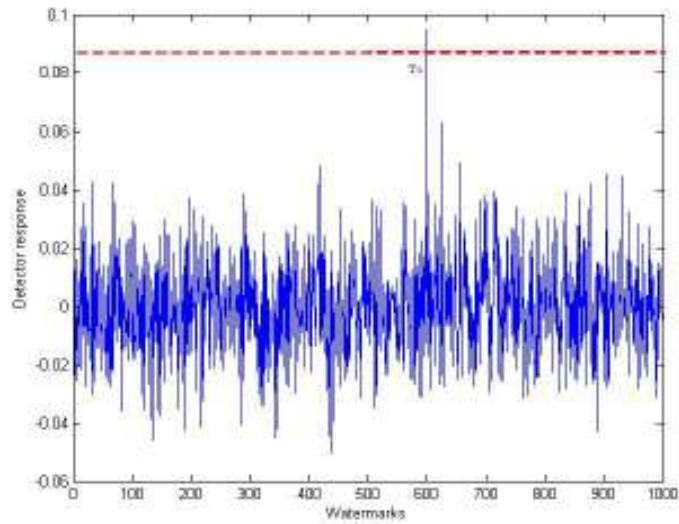
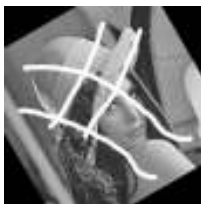


Fig. 7. Corrupted "Lena" and the detector response of embedded watermark

## 5. CONCLUSION

This paper proposed a method for transparently and robustly embedding a watermark into the curvelet transform of grayscale images. We embed the watermark into the selected blocks, scale and curvelet coefficients based on the edge map of the cover image. The embedding strength is adjusted by a Just Noticeable Distortion (JND) model computed for each curvelet coefficient. Robustness is tested against a variety of types of image attacks. Since the curvelet transform enables most of the energy of the object to be localized in just a few coefficients, the optimally sparse representations of image edges allows for the embedded watermarks to recover from severe image degradation. Moreover, the edge map combined with radon transform serves as an essential step to synchronize the embedding location in the content, which makes our proposed algorithm provide robustness against geometric attacks as well. The selected threshold for watermark detection is determined on the statistical analysis over the host signals and embedding schemes. Experiments show our scheme is capable of keeping the probability of false positive low and is generally robust against a wide range of image attacks.

## REFERENCES

- <sup>1</sup> J.J.K. Ó Ruanaidh, W.J. Dowling, and F.M. Boland, "Watermarking Digital Images for Copyright Protection," *IEEE Proceedings on Vision, Signal and Image Processing*, 143(4), August 1996, pp. 250-256.
- <sup>2</sup> G. I. J. Cox, M. L. Miller, and J. A. Bloom, "Digital Watermarking," *Morgan Kaufmann Publishers*, 2002.
- <sup>3</sup> A. M. Eskicioglu and E. J. Delp, "Overview of Multimedia Content Protection in Consumer Electronics Devices," *Signal Processing: Image Communication*, Vol. 16, No. 7, pp. 681-699, April 2001.
- <sup>4</sup> B. Furht and D. Kirovski, *Multimedia Watermarking Techniques and Applications*, Auerbach Publications © 2006.
- <sup>5</sup> Chun-Shien Lu, *Multimedia Security: Steganography and Digital Watermarking Techniques for Protection of Intellectual Property*, IGI Publishing © 2005.
- <sup>6</sup> D. Kundur and D. Hatzinakos, "Digital Watermarking Using Multiresolution Wavelet Decomposition," *Proceedings of the 1998 IEEE International Conference on Acoustics, Speech, and Signal Processing (ICASSP 1998)*, Vol. 5, Seattle, Washington, USA, May 12-15, 1998, pp. 2969-2972.
- <sup>7</sup> A. Lumini and D. Maio, "A Wavelet-Based Image Watermarking Scheme," *The International Conference on Information Technology: Coding and Computing (ITCC'00)*, Las Vegas, NV, March 27 - 29, 2000, pp. 122-127.
- <sup>8</sup> W. Zhu, Z. Xiong and Y.-Q. Zhang, "Multiresolution Watermarking for Images and Video," *IEEE Transactions on Circuits and Systems for Video Technology*, 9(4), June 1999, pp. 545-550.
- <sup>9</sup> P. Tao and A. M. Eskicioglu, "A Robust Multiple Watermarking Scheme in the DWT Domain," *Optics East 2004 Symposium, Internet Multimedia Management Systems V Conference*, Philadelphia, PA, October 25-28, 2004, pp. 133-144.
- <sup>10</sup> J. Canny, "A computational approach to edge detection", *IEEE Trans. on Pattern Analysis and Machine Intelligence*, 8(6), pp679-698 (1986).
- <sup>11</sup> J. J. K. O'Ruanaidh, and T. Pun, "Rotation, Scale and Translation Invariant Digital Image Watermarking," *Proceedings of International Conference on Image Processing*, 1997, Vol. 1, pp. 536-539.
- <sup>12</sup> E. J. Candès and D. L. Donoho. "Curvelets – a surprisingly effective nonadaptive representation for objects with edges," In C. Rabut A. Cohen and L. L. Schumaker, editors, *Curves and Surfaces*, pages 105-120, Vanderbilt University Press, 2000. Nashville, TN.
- <sup>13</sup> E. J. Candès and D. L. Donoho., "New tight frames of curvelets and optimal representations of objects with piecewise-C2 singularities," *Comm. on Pure and Appl. Math.* 57 (2004), 219-266.
- <sup>14</sup> E. J. Candès and F. Guo, "New multiscale transforms, minimum total variation synthesis: application to edge-preserving image reconstruction," *Sig. Process.*, special issue on Image and Video Coding Beyond Standards 82 (2002), 1519-1543.
- <sup>15</sup> E. J. Candès, L. Demanet, D. L. Donoho, and L. Ying, "Fast Discrete Curvelet Transforms," *Society for Industrial and Applied Mathematics: Multiscale Modeling & Simulation*, 2006, Volume 5 Issue 3, Pages 861-899.
- <sup>16</sup> E. J. Candès and D. L. Donoho, "Ridgelets: the key to higher-dimensional intermittency?" *Phil. Trans. R. Soc. Lond. A.* 357 (1999), 2495-2509.
- <sup>17</sup> P.G. Barten, "Evaluation of subjective image quality with the square-root integral method," *Journal of Optical Society of America*, 7(10), 2024-2031, 1990, October.

- <sup>18</sup> A. B. Watson, editor. *Digital Images and Human Vision*. Cambridge, MA: MIT Press, 1993.
- <sup>19</sup> S. Daly, "The Visible Difference Predictor: An Algorithm for the Assessment of Image Fidelity," in A. B. Watson, editor, *Digital Images and Human Vision*, Chapter 14, pp. 179–206. Cambridge, MA: MIT Press, 1993.
- <sup>20</sup> J. Lubin. "The Use of Psychophysical Data and Models in the Analysis of Display System Performance," in A. B. Watson, editor, *Digital Images and Human Vision*, pp. 163–178. Cambridge, MA: MIT Press, 1993.
- <sup>21</sup> C. J. van den Branden Lambrecht and J. E. Farrell. "Perceptual Quality Metric for Digitally Coded Color Images," *Proceedings of EUSIPCO*, pp. 1175–1178, 1996.
- <sup>22</sup> P.G. Barten, "Evaluation of subjective image quality with the square-root integral method," *Journal of Optical Society of America*, 7(10), 2024-2031, 1990, October.
- <sup>23</sup> S. Daly, "The visible differences predictor: An algorithm for the assessment of image fidelity", *SPIE, Human Visual Processing, and Digital Display*, vol.1666,No.3, pp.2- 15, 1992.
- <sup>24</sup> P. Toft, "The Radon Transform - Theory and Implementation", Ph.D. thesis, Department of Mathematical Modelling, Technical University of Denmark, June 1996.
- <sup>25</sup> C. Lian and D. Sidan, "Rotation, scale and translation invariant image watermarking using Radon transform and Fourier transform," *Emerging Technologies: Frontiers of Mobile and Wireless Communication*, 2004.